CONTRAST MEDIA & MOLECULAR IMAGING

Received: 24 April 2013, Revised: 13 June 2013, Accepted: 2 July 2013, Published online in Wiley Online Library

(wileyonlinelibrary.com) DOI: 10.1002/cmmi.1558

Generation and characterization of nanobodies targeting PSMA for molecular imaging of prostate cancer

Mehdi Evazalipour[a,b†], Matthias D'Huyvetter[c,l†], Bahram Soltani Tehrani[d], Mohsen Abolhassani[a]*, Kobra Omidfar[e], Shahriyar Abdoli[f], Roghaye Arezumand[g], Hamid Morovvati[h], Tony Lahoutte[c,i], Serge Muyldermans[j,k] and Nick Devoogdt[c]

Nanobodies show attractive characteristics for tumor targeting in cancer diagnosis and therapy. A radiolabeled nanobody binding the prostate-specific membrane antigen (PSMA) could offer a noninvasive strategy to select prostate cancer patients eligible for PSMA-targeted therapies. We here describe the generation, production and *in vivo* evaluation of anti-PSMA nanobodies. Nanobodies were derived from heavy-chain-only antibodies, raised in immunized dromedaries. Binding characteristics were evaluated through ELISA and flow cytometry. Selected nanobodies were radiolabeled with ^{99m}Tc at their hexahistidine tail, after which cell binding capacity and internalization were evaluated on PSMA^{pos} LNCaP and PSMA^{neg} PC3 cell lines. *In vivo* tumor targeting was analyzed in both LNCaP and PC3 xenografted mice through SPECT/microCT and tissue sampling. A panel of 72 generated clones scored positive on ELISA, all contributing to three nanobody groups, of which group 3 dominated with 70 clones. ELISA and FACS analysis led to the selection of two dominant nanobodies. ^{99m}Tc-labeled PSMA6 and PSMA30 both showed specific binding on LNCAP cells, but not on PC3 cells. ^{99m}Tc-PSMA30 internalized significantly more in LNCaP cells compared to ^{99m}Tc-PSMA6. Higher absolute tumor uptake and tumor-to-normal organ ratios were observed for ^{99m}Tc-PSMA30 compared with ^{99m}Tc-PSMA6 and a ^{99m}Tc-control nanobody in LNCaP but not in PC3 tumor-bearing mice. PSMA30 nanobody has improved targeting characteristics both *in vitro* as well as *in vivo* compared with PSMA6 and the control nanobody, and was therefore selected as our in-house-developed lead compound for PSMA targeting. Copyright © 2014 John Wiley & Sons, Ltd.

Keywords: PSMA; nanobody; imaging; antibody fragment

1. INTRODUCTION

Prostate cancer (PCa) is the most common cancer in men. When detected in an early stage, the 5-year survival rate is nearly 100%. Once the cancer has spread outside the prostate, the survival rate decreases significantly (1). Consequently, early detection of prostate cancer is of upmost importance. Nowadays serum PSA (prostate-specific antigen) kinetics are followed as a routine laboratory test, but it has been known to be unreliable for active

* *Correspondence to: M. Abolhassani, Department of Immunology, Pasteur Institute of Iran, Tehran, Iran. E-mail: mabolhassani@yahoo.com*

† *The first two authors contributed equally.*

a *M. Evazalipour, M. Abolhassani*
Department of Immunology, Pasteur Institute of Iran, Tehran, Iran

b *M. Evazalipour*
Department of Pharmaceutical Biotechnology, School of Pharmacy, Guilan University of Medical Sciences, Rasht, Iran

c *M. D'Huyvetter, T. Lahoutte, N. Devoogdt*
In vivo Cellular and Molecular Imaging Laboratory, Vrije Universiteit Brussel, Brussels, Belgium

d *B. S. Tehrani*
Cellular and Molecular Research Center, Faculty of Medicine, Guilan University of Medical Sciences, Rasht, Iran

e *K. Omidfar*
Biosensor Research Center, Endocrinology and Metabolism Molecular-Cellular Sciences Institute, Tehran University of Medical Sciences, Tehran, Iran

f *S. Abdoli*
Department of Virology, Pasteur Institute of Iran, Tehran, Iran

g *R. Arezumand*
Department of Molecular Medicine, Pasteur Institute of Iran, Tehran, Iran

h *H. Morovvati*
Animal Facility, Guilan University of Medical Sciences, Rasht, Iran

i *T. Lahoutte*
Nuclear Medicine Department, UZ Brussel, Brussels, Belgium

j *S. Muyldermans*
Cellular and Molecular Immunology Unit, Vrije Universiteit Brussel, Brussels, Belgium

k *S. Muyldermans*
Department of Structural Biology, VIB, Brussels, Belgium

l *M. D'Huyvetter*
Radiobiology Unit, Molecular and Cellular Biology Expert Group, Belgian Nuclear Research Center (SCK•CEN), Mol, Belgium

surveillance (2). Repeat biopsies are used to obtain information on tumor presence, size and grade, contributing to the decision to start treatment. However, it remains unclear what Gleason score or tumor size justifies treatment (3). When PSA levels reach 2 ng/ml, radiation therapy has been shown to be ineffective after prostatectomy. PET-imaging with ^{18}F- and ^{11}C-labeled choline is used routinely, but has difficulty identifying lesions in patients with blood PSA levels $<$2.5 ng/ml (4,5). In addition, ^{11}C-acetate also exhibits limited potential in patients with low blood PSA levels (6). In this regard, inconsequent staging of the disease often leads to overtreatment, which has an important impact on the quality of life of men with prostate cancer (7). Moreover, diagnostics that are able to image lesions at low PSA levels are of great interest.

A noninvasive method within PCa diagnostics could offer a new, more convenient tool to select the most appropriate treatment for prostate cancer patients. An emerging target for noninvasive diagnosis of PCa is the prostate-specific membrane antigen (PSMA). This 750-amino acid type II transmembrane protein, with a glutamate-carboxypeptidase activity and a molecular weight of about 110 kDa (8–11), is over-expressed on PCa cells, especially in advanced stage PCa, and shows low expression in normal human tissue (12). The extracellular domain of PSMA is an attractive target for high-contrast nuclear imaging probes.

PSMA was initially approved as a diagnostic target using the radiolabeled monoclonal antibody (mAb) 7E11 (ProstaScint®) (13). The efficacy of ProstaScint® has been reported in several studies, with an average sensitivity of 60%, a positive predictive value of 60%, and a negative predictive value of 70% (14). As it recognizes an internal epitope of the PSMA receptor, its utility is limited to necrotic tumors (15). Recently, several new antibodies directed against PSMA have been introduced into pre-clinical and clinical studies (16–20), of which the mAb, referred to as J591, has shown great potential for *in vivo* PSMA targeting (21,22). However, because of the long circulating half-life of radiolabeled antibodies, it takes several days to acquire high contrast images with PET or SPECT imaging (23).

Small-molecule urea-based inhibitors targeting PSMA recently emerged as most-suitable tracers for imaging PSMA-expressing PCa. For instance, ^{123}I-MIP-1072 and ^{123}I-MIP-1095 are able to detect small lesions as early as 1–4 h post-injection (p.i.), using SPECT-CT in men with metastatic PCa (24). A ^{68}Ga-labeled PSMA inhibitor showed great potential in imaging small metastases that were not picked up by ^{18}F-choline (25).

An emerging strategy in developing high-contrast nuclear imaging probes is the use of a special type of antibody fragment, called a nanobody. Nanobodies are the antigen-binding fragments from heavy chain-only antibodies (HcAbs), derived from *camelidae*. Nanobodies generated against EGFR, CEA and HER2 (26–28) have been described previously. Because of their small size (MW $<$ 15 kDa) and their general characteristics (29), they have important properties that make them suitable for the molecular imaging of tumors. In this manuscript we describe the generation and production of nanobodies directed against PSMA. Selected nanobodies were radiolabeled with 99 m-Technetium (^{99m}Tc). Cell binding and cell internalization were confirmed on PSMA^{pos} LNCaP and PSMA^{neg} PC3 cell lines. *In vivo* biodistribution was evaluated in PSMA^{pos} and PSMA^{neg} tumor-bearing xenografts through SPECT/micro-CT imaging and tissue sampling.

2. RESULTS

2.1. Generation of anti-PSMA Nanobodies

Two dromedaries were immunized with three sources of human PSMA: LNCaP cells, a peptide corresponding to a surface-exposed epitope on the extracellular domain and a recombinant PSMA extracellulair domain protein (30). ELISA analysis of mixed serum samples on immobilized recombinant human PSMA protein before and during the immunization schedule confirmed the generation of an anti-PSMA humoral response (Fig. 1A). Blood from immunized animals was used to construct an immune nanobody library. Nanobodies were phage-displayed and used in biopanning experiments. After three rounds of pannings and ELISA screenings on recombinant PSMA protein, a total of 72 clones out of $>$500 screened scored positive and were sequenced. A sequence similarity tree reveals the presence of three nanobody groups, of which group 3 dominated with 70 clones (Fig. 1B). Nanobodies PSMA20, PSMA32, PSMA6 and PSMA30 were selected for further analysis, of which the latter dominated the nanobody panel with a 33% frequency. Selected nanobodies were purified as hexahistidine-tagged ~15 kDa proteins to $>$95% homogeneity (Fig. 1C).

2.2. Evaluation of PSMA-Binding Potential

ELISA experiments with selected nanobodies at saturating concentrations of 650 nM (10 μg/ml) showed that all bound recombinant PSMA protein (Fig. 2A, $p < 0.001$ for all vs no antigen). These ELISA signals were due to specific interactions of nanobodies to immobilized PSMA, since background signals were obtained when an HER2 recombinant protein was immobilized (Fig. 2A). Nanobody PSMA20 showed elevated background signals, possibly owing to aspecific interactions of nanobody with overcoat or plastic.

Next, affinities of nanobodies towards their target antigen were estimated via saturation ELISA binding studies. The example of PSMA32 is shown in Fig. 2(B). Figure 2(C) summarizes the affinities of all investigated nanobodies to recombinant PSMA antigen, with PSMA30 and PSMA20 showing equally good affinities around 4.5 nM and PSMA32 and PSMA6 showing 2- to 8-fold lower binding potential, respectively.

Finally, nanobody binding to the PSMA receptor was assessed in flow cytometry studies. As shown in Fig. 3(A), both PSMA30 and PSMA6, but not a control nanobody, bound to PSMA^{pos} LNCaP prostate cancer cells. Surprisingly, also PSMA20 and PSMA32 were unable to bind the PSMA receptor. None of the tested nanobodies bound to PSMA^{neg} PC3 prostate cancer cells (Fig. 3B).

2.3. Specificity of ^{99m}Tc-labeled anti-PSMA Nanobodies

For both conditions (using adherent/fixed or nonadherent/nonfixed tumor cells), binding of ^{99m}Tc-labeled PSMA30 and PSMA6 at K_D concentrations, and a control nanobody was presented as total binding vs blocking with a 500-fold excess of cold nanobody on PSMA^{pos} LNCaP cells and vs binding on PSMA^{neg} PC3 cells, as illustrated in Fig. 4. Significant blocking of binding occurred for both PSMA30 and PSMA6 ($p < 0.01$). No specific binding was observed on PC3 cells. The control nanobody only showed some aspecific binding on both LNCaP and PC3 cells.

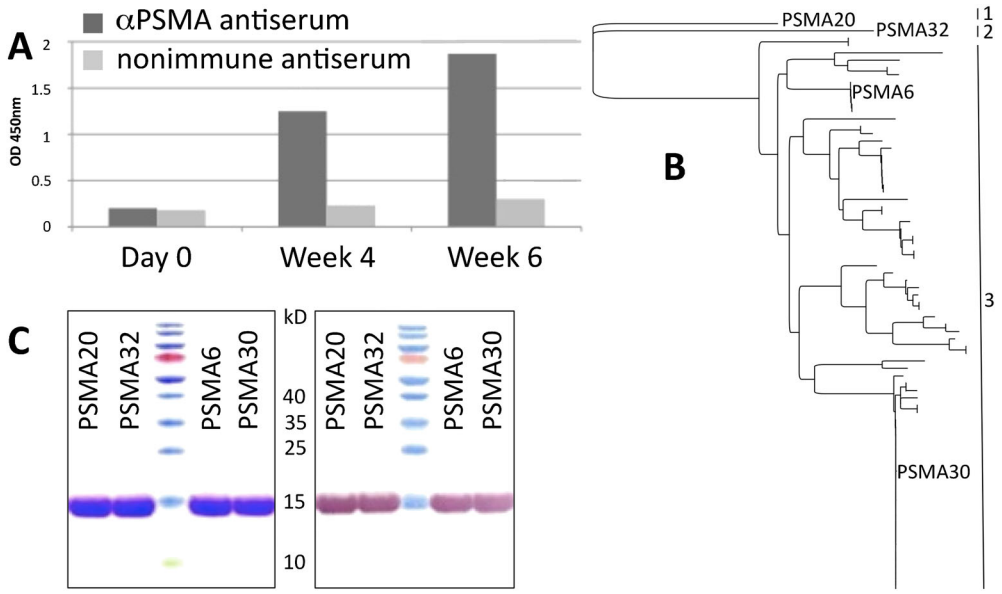

Figure 1. Generation and purification of anti-prostate-specific membrane antigen (PSMA) nanobodies. (A) ELISA of nonimmune serum and serum from dromedaries before and at two time-points after immunization showed the generation of antibodies binding to recombinant human PSMA protein. (B) Phylogenetic tree showing sequence similarities among 72 nanobodies identified after phage display and ELISA screenings to bind to recombinant PSMA protein. Three large sequence groups could be discriminated, among which four nanobodies were selected for further analyses. (C) reducing SDS–PAGE (left panel) and western blot with an anti-His antibody (right panel) showed the purity and hexahistidine-tagged nature of produced nanobodies.

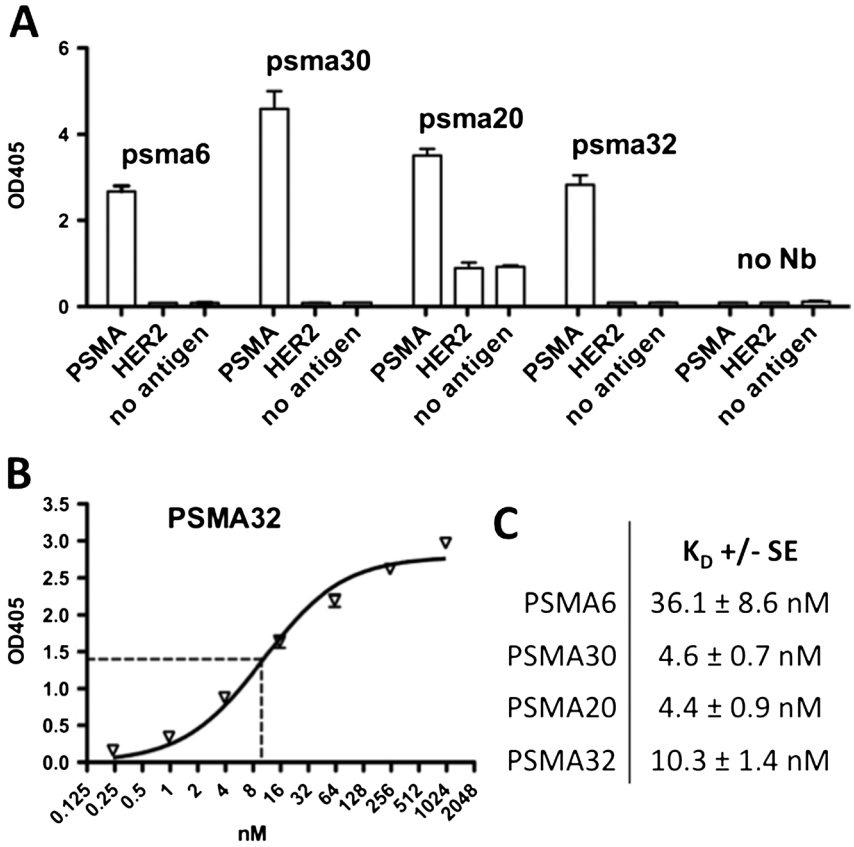

Figure 2. Selected nanobodies specifically bind to recombinant PSMA protein with high affinities. (A) ELISA showing all nanobodies bind to recombinant PSMA, but not recombinant HER2. (B) ELISA of a 4-fold dilution series of PSMA32 showing saturation binding to recombinant PSMA protein. Equilibrium dissociation constants K_D values (a measurement of affinity) were determined via nonlinear regression as the concentration at which half-maximal signals were obtained, and are summarized in (C).

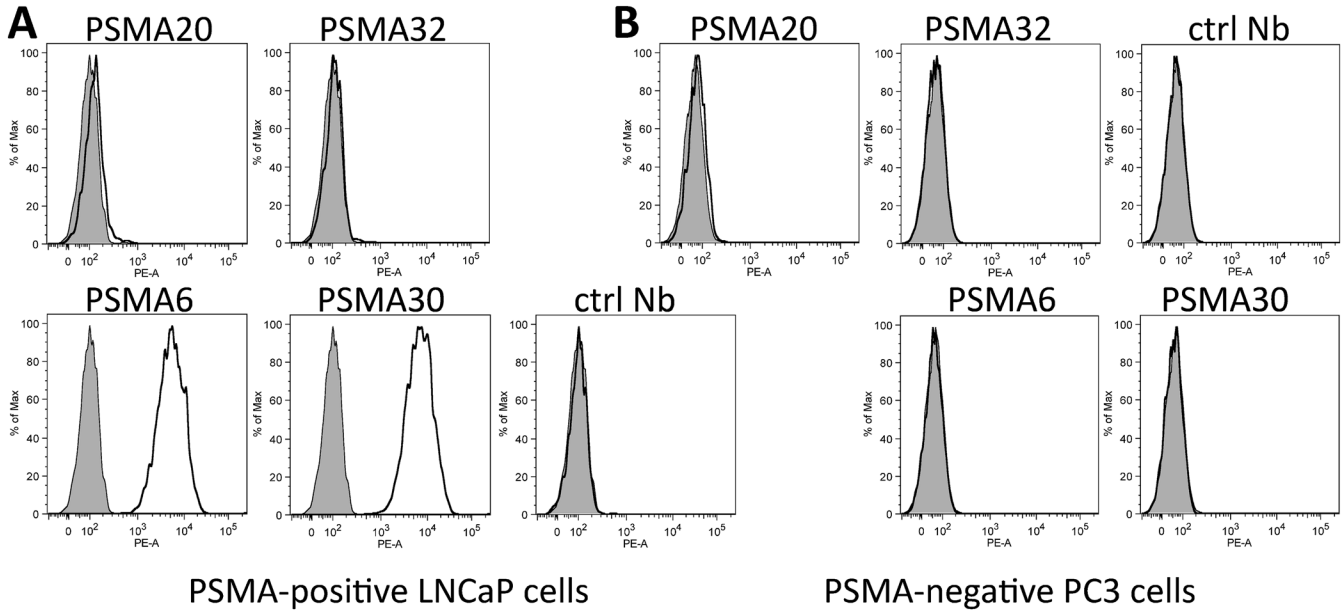

Figure 3. Flow cytometry analysis of selected nanobodies. Binding of PSMA20, PSMA32, PSMA6, PSMA30 and a control nanobody to PSMA-positive LNCaP (A) and PSMA-negative PC3 cells (B) are shown as unstained histograms and compared with background signals (in the absence of nanobody, grey histograms). *x*-Axis: fluorescence intensities; *y*-axis: percentage of maximum signal.

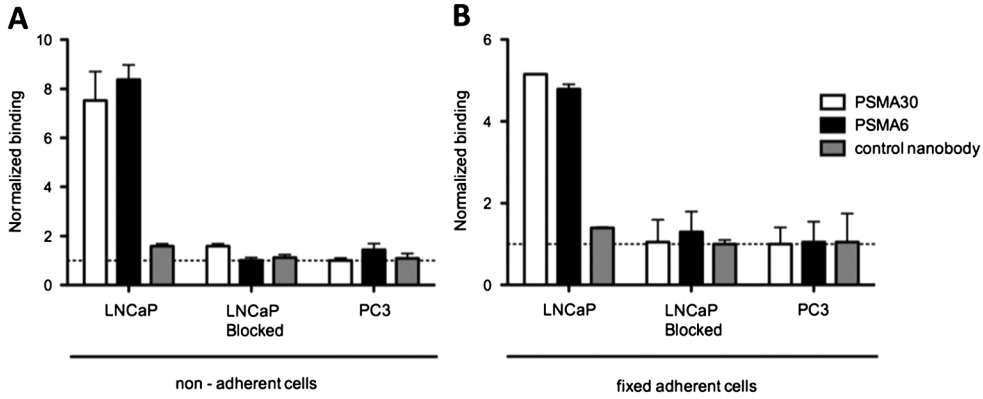

Figure 4. Specificity of the ^{99m}Tc-labeled nanobodies. Binding of 20 nM PSMA30, PSMA6 and control nanobody on PSMA-positive LNCaP and PSMA-negative PC3 cell line in nonadherent/nonfixed (A) and adherent/fixed (B) conditions. Specific competition was achieved with a 500× molar excess of cold nanobody (blocked). Data are presented as fold higher binding as compared with binding of control nanobody to PC3 cells. Note the specific binding of both PSMA30 and PSMA6 on the PSMA-positive LNCaP cell line.

2.4. Internalization of ^{99m}Tc-labeled anti-PSMA Nanobodies

Figure 5 shows the relative amount of radioactivity accounted as membrane-bound, internalized and released in supernatant, for both ^{99m}Tc-PSMA30 and PSMA6 at different time points. In general, the highest amount of radioactivity was measured in the supernatant fractions, with about 90% of the initial bound activity for PSMA6 and around 75% for PSMA30, at all time points. For the membrane-bound fraction, values $<$10% for PSMA6 and around 10% for PSMA30 were obtained at all time points. Values $<$10% for PSMA6 and around 18% of initial bound activity for PSMA30 were measured in the internalized fraction at all timepoints. Cell-associated activity (sum of membrane-bound fraction and the internalized fraction) was significant higher for PSMA30 compared with the values obtained for PSMA6.

2.5. Single pinhole SPECT/micro-CT of ^{99m}Tc-labeled anti-PSMA Nanobodies

Images were successfully gathered 1 h after i.v. injection of ^{99m}Tc-PSMA30 and PSMA6, and the control nanobody in LNCaP and PC3 xenografts. As shown in Fig. 6, specific tumor targeting using PSMA30 was achieved. Low activities in nontarget organs were measured, together with intense activity in the kidneys and bladder, which is a known characteristic of small radiolabeled proteins and peptides. Quantification of the radioactive signals in the LNCaP xenografts via AMIDE software gave rise to tumor-to-muscle (T/M) ratios of 17 ± 5.60, 2.17 ± 0.42 and 1.7 ± 0.26, while in PC3 xenografts values of 1.2 ± 0.13, 1.0 ± 0.34 and 1.8 ± 0.4 were obtained for PSMA30, PSMA6 and control nanobody, respectively, which is in agreement to the *ex vivo* data (see below).

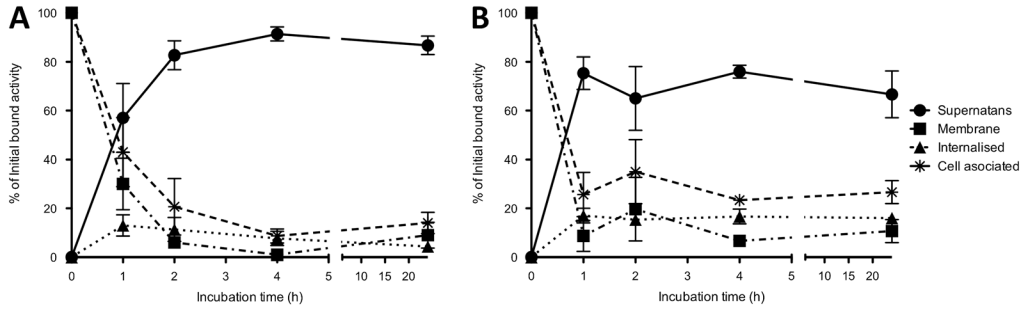

Figure 5. Internalization of the ^{99m}Tc-labeled PSMA nanobodies. Internalization of (A) PSMA6 and (B) PSMA30 on the PSMA-positive LNCaP cell line. Each graph represents different fractions (membrane bound/internalized/supernatant) at 0, 1, 2, 4 and 24 h incubation, expressed as a percentage of initial bound activity. Cell-associated fraction is considered the sum of membrane bound + internalized fraction. Note the higher internalization and thus cell-associated fraction for PSMA30 vs PSMA6.

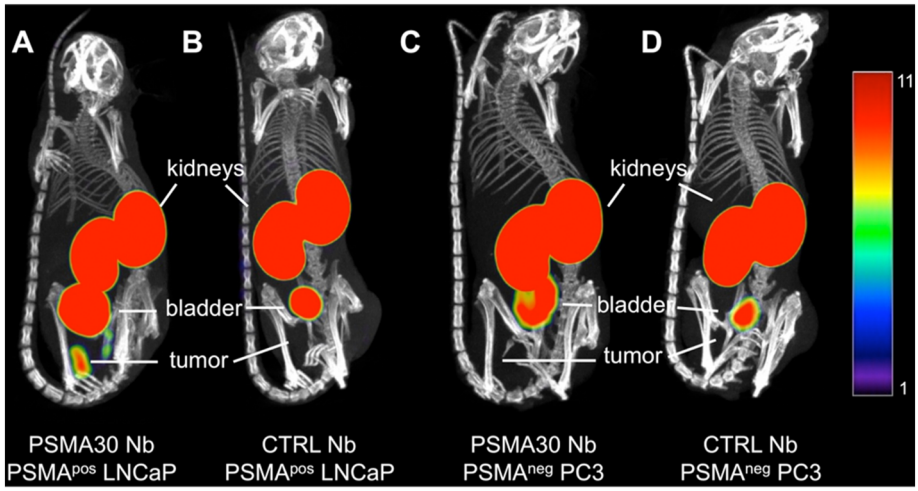

Figure 6. Single pinhole SPECT/micro-CT of the ^{99m}Tc-labeled nanobodies. Fused SPECT/micro-CT images of PSMA-positive LNCaP and PSMA-negative PC3 tumor xenografts, 1 h after i.v. injection of ^{99m}Tc-labeled PSMA30 and control nanobody, with (A) PSMA30 in LNCap xenograft, (B) control nanobody in LNCaP xenograft, (C) PSMA30 in PC3 xenograft and (D) control nanobody in PC3 xenograft. Note the good tumor targeting by PSMA30 in the PSMA-positive LNCaP model vs low accumulation by the control nanobody.

2.6. *Ex vivo* Biodistribution of ^{99m}Tc-labeled anti-PSMA Nanobodies

After SPECT/CT, the animals were euthanized 90 min p.i., after which tumor and major organs were isolated. Ex vivo measurements in tumor and nontarget organs are summarized in Table 1. Accumulation of radioactivity in the LNCaP tumors was significant higher ($p < 0.005$) for both PSMA30 and PSMA6, with $1.57 \pm 0.36\%$ and $0.43 \pm 0.08\%$ IA/g, compared with the control nanobody (uptake value of $0.18 \pm 0.01\%$ IA/g). Moreover, the uptake of PSMA30 was significant higher than that of PSMA6 ($p < 0.01$). In PC3 xenografts, tumor uptake values of 0.15 ± 0.05, 0.34 ± 0.05, $0.36 \pm 0.04\%$ IA/g were measured for PSMA30, PSMA6 and control nanobody, respectively. Kidney uptake was significantly lower for PSMA30, with an uptake value of 85.43 ± 18.82 in the LNCaP xenografts ($p < 0.001$), compared with 148.66 ± 9.56 and $181.69 \pm 17.58\%$ IA/g for PSMA6 control nanobody, which was confirmed in PC3 xenografted mice. High tumor-to-background ratios are of great interest. Figure 7 shows the different tumor-to-organ ratios in LNCaP xenografts for all three nanobodies. PSMA30, which had the highest tumor uptake, showed a tumor-to-muscle (T/M) value of 23.39 ± 5.03 which was significantly higher ($p < 0.001$) compared with the T/M values of both PSMA6 and control nanobody (3.1 ± 0.88 and 1.35 ± 0.13). The tumor-to-blood value of PSMA30 (7.56 ± 2.23) was again significantly higher ($p < 0.01$) than those measured for both PSMA6 and control nanobody (3.1 ± 0.88 and 1.35 ± 0.13).

3. DISCUSSION

There is an urgent need for a sensitive, noninvasive technique for tumor staging and treatment follow-up of PCa. PSMA is highly expressed on prostate cancer cells, which makes it an attractive target for high-contrast nuclear imaging probes. Current available diagnostics, like PET-imaging with ^{18}F/^{11}C-choline and ^{11}C-acetate, have shown low sensitivity at early-stage disease. Ideal tracers for PCa diagnostics should exhibit both good affinities towards target tissue and fast clearance from nontarget organs, leading to high contrast imaging at early time points.

As excellently reviewed by Osborne *et al.* (31), several PSMA-targeting radiotracers have been evaluated in xenografted

Table 1. *Ex vivo* biodistribution uptake values of ^{99m}Tc-labeled nanobodies at 90 min p.i. and expressed as %IA/g. Biodistribution is based on the dissection values (expressed as %IA/g) at 90 min p.i. Data are means ± SD of three mice per nanobody. PSMA6 and PSMA30 were evaluated together with a control nanobody in both PSMA-positive LNCaP and PSMA-negative PC3 xenografts.

	PSMA^{pos} LNCaP			PSMA^{neg} PC3		
Organ/tissue	Control nanobodies	PSMA6	PSMA30	Control nanobodies	PSMA6	PSMA30
Lungs	0.41 ± 0.08	0.4 ± 0.18	0.18 ± 0.09	0.50 ± 0.05	0.46 ± 0.07	0.26 ± 0.07
Heart	0.17 ± 0.03	0.18 ± 0.06	0.09 ± 0.02	0.22 ± 0.02	0.18 ± 0.06	0.07 ± 0.01
Liver	0.58 ± 0.11	0.63 ± 0.16	0.24 ± 0.05	0.32 ± 0.05	0.50 ± 0.05	0.15 ± 0.01
Kidney	181.69 ± 17.58	148.66 ± 9.56	85.43 ± 18.82	138.86 ± 29.32	127.5 ± 24.40	86.9 ± 5.29
Stomach	0.16 ± 0.04	0.25 ± 0.05	0.13 ± 0.01	0.08 ± 0.03	0.20 ± 0.04	0.07 ± 0.04
Spleen	0.15 ± 0.04	0.17 ± 0.02	0.10 ± 0.04	0.15 ± 0.01	0.16 ± 0.05	0.07 ± 0.01
Muscle	0.14 ± 0.02	0.15 ± 0.05	0.07 ± 0.03	0.12 ± 0.02	0.13 ± 0.03	0.05 ± 0.01
Bone	0.36 ± 0.05	0.33 ± 0.14	0.21 ± 0.05	0.21 ± 0.11	0.12 ± 0.03	0.04 ± 0.01
Small intestine	0.15 ± 0.05	0.14 ± 0.04	0.10 ± 0.02	0.22 ± 0.05	0.23 ± 0.04	0.15 ± 0.06
Large intestine	0.17 ± 0.07	0.24 ± 0.12	0.14 ± 0.06	0.14 ± 0.04	0.20 ± 0.06	0.07 ± 0.01
Blood	0.42 ± 0.08	0.41 ± 0.15	0.21 ± 0.03	0.40 ± 0.10	0.46 ± 0.17	0.17 ± 0.02
Lymph nodes	0.19 ± 0.04	0.21 ± 0.13	0.12 ± 0.01	0.21 ± 0.01	0.19 ± 0.07	0.08 ± 0.02
Tumor	0.18 ± 0.01	0.43 ± 0.08	1.57 ± 0.38	0.36 ± 0.04	0.34 ± 0.05	0.15 ± 0.05

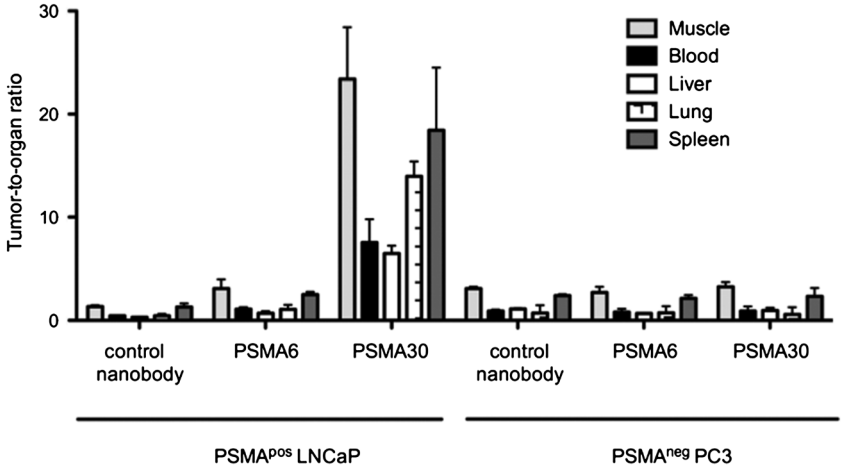

Figure 7. Tumor-to-organ ratios of the ^{99m}Tc-labeled nanobodies. Tumor-to-organ ratios were calculated from the *ex vivo* biodistribution uptake values. Ratios to muscle, blood, liver, lung and spleen were calculated for control nanobody, PSMA6 and PSMA30 in both PSMA-positive LNCaP and PSMA-negative PC3 xenografts. Note the higher ratios obtained for PSMA30 in the PSMA-positive LNCaP xenografts vs both PSMA6 and control nanobody. Low ratios were obtained for all three nanobodies on the PSMA-negative PC3 xengrafts.

prostate cancer mouse models and some already have even been tested in patients. Basically, the evaluated tracers can be divided into two categories: antibodies and small molecules. Small molecule tracers include the peptidomimetics that were described by Eder *et al*. (25), which show high specific uptake in PSMA-expressing tumors (~7% IA/g at 1 h p.i.), fast excretion and good contrast images early after administration (T/M ≈ 4 at 1 h p.i.). Tracers derived from full antibodies are not very well suited to diagnostic imaging applications since, owing to their slow blood and tissue clearance, their ability to generate reliable antigen-specific contrast images is suboptimal. For instance, although uptake of anti-PSMA antibodies in PSMA-positive tumors is high (5–20% IA/g), uptake of irrelevant antibody in the same tumors is only 2- to 3-fold lower (18). Blood clearance of these antibodies has also been reported to be so slow that tumor-to-blood ratios are <2, at 2 to 4 days p.i. (18). Hence, same-day imaging with low radiation burden is not possible with tracers derived from full-sized antibodies. In an attempt to decrease blood half-life, smaller antibody-fragments such as scFvs binding PSMA with high affinities have recently been generated (32), but their usefulness for diagnostic nuclear imaging still needs to be determined.

In the present study we describe the generation and characterization of nanobodies directed against PSMA. Nanobodies are the smallest possible functional antibody derivatives that combine high affinities with fast blood clearance and good tumor targeting to generate high contrast images early after systemic administration (29). Four nanobodies PSMA20, PSMA32, PSMA6 and PSMA30 were selected for further analysis, of which the latter dominated the selected nanobody panel by a 33% frequency. All four were tested on their binding to recombinant PSMA, and nanomolar affinities were estimated through ELISA. Flow cytometry revealed no significant binding on the PSMA^{pos} LNCaP cell line for nanobodies PSMA20 and PSMA32, leaving

both out for further analysis. Subsequently, PSMA30 and PSMA6 were radiolabeled with ^{99m}Tc, and further tested for specific cell binding and internalization. Specific binding on LNCaP cells was observed for both PSMA nanobodies, which was reduced significantly by adding a 500-fold molar excess of unlabeled nanobody. No binding was observed on PC3 cells. PSMA30 showed a significantly higher degree of internalization and thus a higher cell-associated fraction compared with PSMA6, which is of great interest for therapeutic applications where entrapment of therapeutic radionuclides is of importance. The degree of internalization is in agreement with previously conducted internalization assays using monovalent nanobodies targeting other cancer-specific antigens. In general our obtained values are low, which might be caused by an early dissociation from the PSMA-receptor prior to receptor-mediated endocytosis. Consequently, less nanobody (and thus radiolabel) is internalized inside the tumor cells. Compared with a recent report on the urea-based compounds [^{123}I]MIP-195 and [^{123}I]MIP-1072 (33), we observe a 2.5-fold lower degree of internalization. However, a direct comparison is difficult since the radiolabel (and thus the radiochemistry) was different. To select the anti-PSMA nanobody with the highest potential as a high contrast nuclear probe, the *in vivo* biodistribution was evaluated in both LNCaP and PC3 tumor-bearing xenografts. SPECT/micro-CT images were taken 1 h p.i., followed by tissue sampling at 90 min p.i. Optimal tumor-to-organ ratios are of upmost importance, since high contrast images at early time points are desirable. In the LNCaP tumor xenografts, significantly higher tumor uptake values were measured for both PSMA30 and PSMA6 ($p < 0.005$) compared with the control nanobody. However, the uptake values of PSMA30 were significant higher than those measured for PSMA6 ($p < 0.01$), which is in agreement with its better affinity and higher internalization potential. In the PC3 xenografts, no significant differences were observed in tumor uptake values between all three nanobodies. Calculated tumor-to-organ values for PSMA30 were very high in the LNCaP xenografts, and were higher compared with the ratios obtained for PSMA6 and control nanobody. Although the absolute uptake values in PSMA^{pos} tumors of PSMA30, at 1 h p.i. are lower compared with, for instance, urea based-compounds, the obtained target-to-nontarget tissue ratios are in close accordance.

^{99m}Tc-labeled Nanobodies have been shown to be very specific, with low accumulation in nontarget tissue. However, as compared with the described anti-PSMA nanobodies showing specific tumor targeting values of 1.6%IA/g, tumor uptake of HER2, EGFR or CEA-targeting nanobodies in respective tumor models is usually higher (4–10% IA/g) (26–28). Possible explanations for the lower absolute uptake of anti-PSMA nanobodies could be the less optimal affinity parameters or internalization rates, a lower PSMA expression level in the tumor or differences in tumor vasculature.

All ^{99m}Tc-labeled nanobodies described in this study accumulate intensely in the kidneys. This is a well-described phenomenon typical for small charged proteins and peptides, and is also observed with additional PSMA-targeting small molecules (31). It is explained by a fast clearance through the glomerulus and a subsequent, nonspecific reuptake in the proximal tubuli. Moreover, several reports confirmed the presence of PSMA in mouse kidney, which could also contribute to this accumulation (34). So far it remains unclear to what extent the retention is caused by specific interaction with PSMA receptors present in the renal tissue. Nevertheless, these high kidney signals could interfere with the imaging of the prostate, and moreover the metastases in the proximity of the kidneys. In this study, we observed a significantly lower kidney retention of PSMA30 compared with both PSMA6 and control nanobody ($p < 0.001$). Moreover, we recently showed that removing the hexahistidine tail lowers kidney retention by >50%, without affecting tumor-targeting properties (35). In the current study we labeled nanobodies site-specifically with ^{99m}Tc and used them for SPECT/CT imaging to generate a proof-of-concept of PSMA tumor targeting in mice. In further steps we will optimize labeling strategies for the selected lead nanobody PSMA30. The most evident choice would be to couple with the bifunctional chelator NOTA and to label with the radionuclide ^{68}Ga for use in PET imaging. Using these settings, we have shown previously that the optimal breast tumor targeting properties of a HER2-targeting nanobody are maintained, that the generated tracer shows a good toxicology profile in animals and that injected mice receive a relatively low radiation burden (35). A phase I study with the ^{68}Ga-NOTA-anti-HER2 nanobody is ongoing to further evaluate safety and efficacy in patients.

4. CONCLUSION

The small, antibody-derived, nanobody PSMA30 was selected as a lead compound for further PCa imaging studies, based on the following criteria: (1) high production yields; (2) good affinity; (3) specific recognition of cell-expressed PSMA both under unlabeled and ^{99m}Tc-labeled format; (4) efficient internalization (~18% after 1 h) into PSMA-expressing cells; (5) fast clearance and relatively high (1.6% IA/g) uptake in PSMA-positive tumors and ~5-fold lower levels in PSMA-negative tumors, generating high tumor-to organ ratios (T/M ≈ 23 and T/B ≈ 8) and high-contrast images already at 1 h p.i. These characteristics are optimal for future application of PSMA30 in clinical routine and much better than those of full antibody-derived tracers.

5. EXPERIMENTAL

5.1. Cell line and Culture Conditions

The PSMA^{pos} LNCaP human prostate carcinoma cell line and the PSMA^{neg} PC3 prostate adenocarcinoma cell line were obtained from the Health Protection Agency Culture Collection (Salisbury, UK). LNCaP cells were cultured using RPMI 1640 medium, PC3 cells in Coons Modified Ham's F12 medium. All media were enriched with 10% fetal bovine serum, 2 mM Glutamine, 100 U/ml penicillin and 0.1 mg/ml streptomycin. RPMI 1640 was also enriched with 1.0 mM sodium pyruvate. Cells were grown in a humidified atmosphere with 5% CO_2 at 37 °C. Cells were detached by using trypsin–EDTA. Media and supplements were obtained from Invitrogen (Paisley, UK).

5.2. Dromedary Immunization and Immune Response

The generation of an anti-human PSMA antibody immune response in dromedaries is described elsewhere (30). Briefly, animals were immunized with LNCaP cells, a 28-amino acid PSMA peptide and recombinant human PSMA protein. The immune response was monitored by testing 1000-fold diluted serum samples in ELISA on coated recombinant PSMA (RnD Systems). Bound camel antibodies were detected with polyclonal rabbit anti-camel IgG, followed by HRP-conjugated anti-rabbit-IgG.

5.3. Identification and Production of anti-PSMA Nanobodies

The nanobody immune library was constructed and nanobodies were selected by phage display, as described previously (36). Basically, 3 days after the last immunization, blood was collected and peripheral blood lymphocytes were purified. Total RNA was extracted and DNA fragments encoding nanobodies were amplified by nested PCR. Nanobody DNA fragments were ligated in the phage-display vector pHEN4 and transformed into *E. coli* cells to generate a library of 1.5×10^7 transformants. Nanobodies were phage displayed and biopannings were performed on microtiter plates coated with 10 μg recombinant PSMA. Bound phages were recovered by alkaline elution and reamplified to use in a next round of biopanning. Three rounds of panning were performed. After each round of panning, colonies were randomly picked, and nanobody-containing periplasmic extracts were made. These extracts were used to screen PSMA-specific nanobodies by ELISA on recombinant protein. Positive-scoring clones were sequenced, aligned and displayed as a similarity tree using Geneious software (Biomatters, Auckland, New Zealand).

Nanobodies were expressed as hexahistidine-tagged proteins in a bacterial expression system and purified, as described previously (36). Nanobody BcII10, binding a bacterial enzyme (37), was used as a negative control nanobody in all experiments. Nanobody purity was assessed via reducing SDS–PAGE and western blot analysis with anti-His mAb (AbDSerotec, Oxford, UK) and HRP-conjugated anti-mouse IgG (Sigma-Aldrich, St Louis, MO, USA).

5.4. ELISA Assays

ELISAs were performed as described previously (28). Briefly, immunosorbent plates were coated with recombinant human PSMA or HER2 protein and overcoated, and nanobodies were added for 1 h at room temperature. In the specificity ELISA, nanobodies were applied at a concentration of 650 nM (10 μg/ml). In saturation binding ELISAs, a 4-fold serial dilution series from 1 μM to 0.24 nM was tested. Nanobody binding was detected by sequential 1 h incubations at room temperature with 1 μg/ml anti-His antibody, 1 μg/ml alkaline-phosphatase-coupled anti-mouse IgG antibody and 2 mg/ml phosphatase substrate (both from Sigma-Aldrich). To determine K_D values, OD_{405} signals in function of nanobody concentrations were fit via nonlinear regression and analyzed with GraphPad Prism 5 software (GraphPad, San Diego, CA, USA).

5.5. Flow Cytometry Analysis

Flow cytometry analyses of nanobody binding to cells is performed as described previously (28). PSMA expression or its absence on LNCaP or PC3 cells, respectively, was confirmed using a PE-labeled anti-PSMA antibody (Biolegend, San Diego, CA, USA).

5.6. Animal Studies

Male nu/nu mice (mean weight of about 20 g, 6 weeks) were inoculated subcutaneously in the right hind leg with either 1×10^6 LNCaP or 1×10^6 PC3 cells dissolved a 50/50 mixture of PBS and matrigel. Tumors were grown to reach a volume of 200 mm^3. Anesthesia protocols were described previously (26). The ethical committee of the Vrije Universiteit Brussel approved all animal study protocols.

5.7. ^{99m}Tc Nanobody Labeling

Nanobodies were radiolabeled with ^{99m}Tc at their hexahistidine c-terminal end, as described in detail elsewhere (38). Briefly, $[^{99m}Tc(H_2O)_3(CO)_3]^+$ was synthesized by adding 1 ml of fresh $^{99m}TcO_4^-$ eluate (0.74–3.7 GBq) from a ^{99}Mo–^{99m}Tc generator (Drytec; GE Healthcare) to an Isolink kit (Mallinckrodt Medical BV); the mixture was boiled for 20 min and neutralized with 1 M HCl. Next, a 1 mg/ml nanobody solution in PBS was incubated with $[^{99m}Tc(H_2O)_3(CO)_3]^+$ for 90 min at 52 °C, purified on NAP-5, and passed through a 0.22 μm filter. Quality control was performed using instant-thin layer chromatography with 100% acetone as mobile phase.

5.8. Specificity of ^{99m}Tc-labeled anti-PSMA Nanobodies

Specificity of ^{99m}Tc-labeled PSMA30 and PSMA6 was analyzed on the $PSMA^{pos}$ LNCaP and $PSMA^{neg}$ PC3 cell lines, both under nonadherent/nonfixed and adherent/fixed conditions. For the fixed conditions, 1×10^6 cells were adhered overnight in 24 well plates and washed twice with PBS. Subsequently, cells were incubated with 1 ml prewarmed DMEM incubation medium containing 1% bovine serum albumine (BSA) and 0.5% *N*-2-hydroxyethylpiperazine-*N*′-2-ethanesulfonic acid (HEPES) during 1 h at 37 °C. Next, cells were fixed using 4% paraformaldehyde during 15 min at RT. Then, the cells were incubated with 500 μl prewarmed DMEM incubation medium, containing the anti-PSMA nanobodies at K_D concentration. A nontargeting nanobody was used as a negative control. A 500-fold excess of unlabeled nanobody was added in parallel to assess nonspecific binding. The cells were then incubated for 1 h at 37 °C, after which unbound nanobody was washed away and cells were solubilized with 1 M NaOH at 37 °C during 10 min (twice). For the nonadherent condition, 1×10^6 cells were added to flow cytometry tubes. A similar procedure was followed, except that after each step cells were centrifuged during 5 min at 1500 rpm to separate cells from solution. Cell-associated activity was determined with an automatic gamma counter. These data were plotted in Graphpad Prism (version 5.0b).

5.9. Internalization of ^{99m}Tc-labeled anti-PSMA Nanobodies

The percentage of uptake and internalization of ^{99m}Tc-labeled PSMA30 and PSMA6 was determined on the $PSMA^{pos}$ LNCaP cell line, in nonadherent culture conditions; 1×10^6 cells/tube were placed at 4 °C for 1 h, after which a 20 nM nanobody solution was added at 4 °C for 1 h. A 500-fold excess of unlabeled nanobody was added in parallel to assess aspecific binding. Next, the unbound fraction was collected and the cells were incubated at 37 °C during different incubation times. Then, the supernatans fraction was removed, after which the membrane-bound fraction was collected by an acid wash. Finally, cells were collected with 1 M NaOH. All fractions were counted for radioactivity with an automated gamma counter, and plotted in Graphpad Prism (version 5.0b).

5.10. Single Pinhole SPECT/micro-CT of ^{99m}Tc-labeled anti-PSMA Nanobodies

SPECT/micro-CT was performed 1 h after an intravenous injection of about 37 MBq/1 mCi of ^{99m}Tc-labeled PSMA30 and PSMA6, and a control nanobody ($n = 3$). These procedures have been described before (26). Briefly, Micro-CT imaging was followed by pinhole SPECT on separate systems. Micro-CT was performed using a dual-source CT scanner (Skyscan 1178; Skyscan) with 60 kV and 615 mA at a resolution of 83 mm. Images were reconstructed using filtered backprojection (NRecon; Skyscan). Total body pinhole SPECT was performed 1 h post injection using a dual-head γ-camera (e.cam180; Siemens Medical Solutions), mounted with 2 multipinhole collimators (three 1.5 mm pinholes in each collimator, 200 mm focal length, and 80 mm radius of rotation). Images were acquired over 360° in 64 projections of 10 s into 128×128 matrices, resulting in a total imaging time of 14 min. The SPECT images were reconstructed using an iterative reconstruction algorithm. Tumor-to-tissue ratios were calculated using AMIDE (39). Equally scaled SPECT/CT maximal-intensity projections were generated using OsiriX DICOM viewer software.

5.11. *Ex vivo* Biodistribution of ^{99m}Tc-labeled anti-PSMA Nanobodies

After SPECT/micro-CT, mice were euthanized at 90 min p.i., followed by the isolation of tumors, and major organs and tissues, which were then counted for radioactivity with an automated γ-counter. The amount of radioactivity present in the different organs was expressed as percentage injected activity/gram tissue (% IA/g). These data were further used to calculate tumor-to-background tissue ratios.

5.12. Statistical Analyses

Data on the cellular experiments and the comparative biodistribution were analyzed using the unpaired Student *t*-test with a p-value < 0.05 for significant difference.

Acknowledgments

The project of production of Nanobodies against PSMA is the PhD thesis of Mehdi Evazalipour and was financially supported by Pasteur Institute of Iran, Tehran, Iran. We thank the Cellular and Molecular Immunology department at the Vrije Universiteit Brussel for providing a fellowship for Mehdi Evazalipour to conduct his studies in this research unit. Matthias D'Huyvetter is funded by an SCK•CEN/VUB grant. Tony Lahoutte is a senior clinical investigator of the Research Foundation, Flanders. The research at ICMI is funded by the Belgian State, Nationaal Kankerplan, Vlaamse Liga tegen Kanker and Vlaamse Stichting tegen Kanker. We thank Cindy Peleman for technical assistance.

REFERENCES

1. Brawley OW. Prostate cancer epidemiology in the United States. World J Urol 2012; 30(2): 195–200.
2. Ross AE, Loeb S, Landis P, Partin AW, Epstein JI, Kettermann A, *et al*. Prostate-specific antigen kinetics during follow-up are an unreliable trigger for intervention in a prostate cancer surveillance program. J Clin Oncol 2010; 28: 2810–2816.
3. Park BK, Park JW, Park SY, Kim CK, Lee HM, Jeon SS, *et al*. Prospective evaluation of 3-T MRI performed before initial transrectal ultrasound-guided prostate biopsy in patients with high prostate-specific antigen and no previous biopsy. AJR Am J Roentgenol 2011; 197: W876–881.
4. Giovacchini G, Picchio M, Coradeschi E, Bettinardi V, Gianolli L, Scattoni V, *et al*. Predictive factors of [(11)C]choline PET/CT in patients with biochemical failure after radical prostatectomy. Eur J Nucl Med Mol Imag 2010; 37: 301–309.
5. Husarik DB, Miralbell R, Dubs M, John H, Giger OT, Gelet A, Cservenyàk T, Hany TF. Evaluation of [18 F]-choline PET/CT for staging and restaging of prostate cancer. Eur J Nucl Med Mol Imag 2008; 35(2): 253–263.
6. Albrecht S, Buchegger F, Soloviev D, Zaidi H, Vees H, Khan HG, *et al*. (11)C-acetate PET in the early evaluation of prostate cancer recurrence. Eur J Nucl Med Mol Imag 2007; 34: 185–196.
7. Resnick MJ, Koyama T, Fan KH, Albertsen PC, Goodman M, Hamilton AS, *et al*. Long-term functional outcomes after treatment for localized prostate cancer. New Engl J Med 2013; 368: 436–445.
8. Israeli RS, Powell CT, Corr JG, Fair WR, Heston WD. Expression of the prostate-specific membrane antigen. Cancer Res 1994; 54: 807–811.
9. Chang SS, Gaudin PB, Reuter VE, Heston WDW. Prostate-specific membrane antigen: present and future applications. Urology 2000; 55: 622–629.
10. Sam S, Chang MD. Overview of prostate-specific membrane antigen. Rev Urol 2004; 6: S13–S18.
11. Kinoshita Y, Kuratsukuri K, Landas S, Imaida K, Rovito PM, Wang CY, Haas GP. Expression of prostate specific membrane antigen in normal and malignant human tissues. World J Surg 2006; 30: 628–636.
12. Silver DA, Pellicer I, Fair WR, Heston WD, Cordon-Cardo C. Prostate-specific membrane antigen expression in normal and malignant human tissues. Clin Cancer Res 1997; 3: 81–85.
13. Kahn D, Williams RD, Haseman MK, Reed NL, Miller SJ, Gerstbrein J. Radioimmunoscintigraphy with In-111-labeled capromab pendetide predicts prostate cancer response to salvage radiotherapy after failed radical prostatectomy. J Clin Oncol 1998; 16: 284–289.
14. Apolo AB, Pandit-Taskar N, Morris MJ. Novel tracers and their development for the imaging of metastatic prostate cancer. J Nucl Med 2008; 49: 2031–2041.
15. Troyer JK, Beckett ML, Wright GL Jr. Location of prostate-specific membrane antigen in the LNCaP prostate carcinoma cell line. Prostate 1997; 30(4): 232–242.
16. Milowsky MI, Nanus DM, Kostakoglu L, Vallabhajosula S, Goldsmith SJ, Bander NH. Phase I trial of yttrium-90-labeled antiprostate-specific membrane antigen monoclonal antibody J591 for androgen-independent prostate cancer. J Clin Oncol 2004; 22: 2522–2531.
17. Smith-Jones PM, Vallabhajosula S, Navarro V, Bastidas D, Goldsmith SJ, Bander NH. Radiolabeled monoclonal antibodies specific to the extracellular domain of prostate-specific membrane antigen: preclinical studies in nude mice bearing LNCaP human prostate tumor. J Nucl Med 2003; 44: 610–617.
18. Bander NH, Milowsky MI, Nanus DM, Kostakoglu L, Vallabhajosula S, Goldsmith SJ. Phase I trial of 177lutetium-labeled J591, a monoclonal antibody to prostate-specific membrane antigen, in patients with androgen-independent prostate cancer. J Clin Oncol 2005; 23: 4591–4601.
19. Henry MD, Wen S, Silva MD, Chandra S, Milton M, Worland PJ. A prostate-specific membrane antigen-targeted monoclonal antibody-chemotherapeutic conjugate designed for the treatment of prostate cancer. Cancer Res 2004; 64: 7995–8001.
20. Mays TA, Sarantopoulos J, Tolcher A, *et al*. MDX-070, a human anti-plasma antibody, administered as either a single dose or as multiple doses to patients with hormone-refractory prostate cancer. J Clin Oncol 2006(Meeting Abstracts);24: 14549.
21. Milowsky MI, Nanus DM, Kostakoglu L, Sheehan CE, Vallabhajosula S, Goldsmith SJ, *et al*. Vascular targeted therapy with anti-prostate-specific membrane antigen monoclonal antibody J591 in advanced solid tumors. J Clin Oncol 2007; 25: 540–547.
22. Vallabhajosula S, Goldsmith SJ, Kostakoglu L, Milowsky MI, Nanus DM, Bander NH. Radioimmunotherapy of prostate cancer using 90Y- and 177Lu-labeled J591 monoclonal antibodies: effect of multiple treatments on myelotoxicity. Clin Cancer Res 2005; 11: 7195s–7200s.
23. Bander NH. Technology insight: monoclonal antibody imaging of prostate cancer. Nat Clin Pract Urol 2006; 3(4): 216–225.
24. Barrett JA, Coleman RE, Goldsmith SJ, Vallabhajosula S, Petry NA, Cho S, *et al*. First-in-man evaluation of two high-affinity PSMA-avid small

molecules for imaging prostate cancer. J Nucl Med 2013. doi:10.2967/jnumed.112.111203
25. Eder M, Schäfer M, Bauder-Wüst U, Hull WE, Wängler C, Mier W, Haberkorn U, Eisenhut M. 68Ga-complex lipophilicity and the targeting property of a urea-based PSMA inhibitor for PET imaging. Bioconjug Chem 2012; 23(4): 688–697.
26. Vaneycken I, Govaert J, Vincke C, Caveliers V, Lahoutte T, De Baetselier P, Raes G, Bossuyt A, Muyldermans S, Devoogdt N. In vitro analysis and in vivo tumor targeting of a humanized, grafted nanobody in mice using pinhole SPECT/micro-CT. J Nucl Med 2010; 51(7): 1099–1106.
27. Gainkam LO, Huang L, Caveliers V, Keyaerts M, Hernot S, Vaneycken I, Vanhove C, Revets H, De Baetselier P, Lahoutte T. Comparison of the biodistribution and tumor targeting of two 99mTc-labeled anti-EGFR nanobodies in mice, using pinhole SPECT/micro-CT. J Nucl Med 2008; 49(5): 788–795.
28. Vaneycken I, Devoogdt N, Van Gassen N, Vincke C, Xavier C, Wernery U, Muyldermans S, Lahoutte T, Caveliers V. Preclinical screening of anti-HER2 nanobodies for molecular imaging of breast cancer. FASEB J 2011; 25(7): 2433–2446.
29. Vaneycken I, D'Huyvetter M, Hernot S, De Vos J, Xavier C, Devoogdt N, Caveliers V, Lahoutte T. Immuno-imaging using nanobodies. Curr Opin Biotechnol 2011; 22(6): 877–881.
30. Evazalipour M, Tehrani BS, Abolhassani M, Morovvati H, Omidfar K. Camel heavy chain antibodies against prostate-specific membrane antigen. Hybridoma (Larchmt) 2012; 31(6): 424–429.
31. Osborne JR, Akhtar NH, Vallabhajosula S, Anand A, Deh K, Tagawa ST. Prostate-specific membrane antigen-based imaging. Urol Oncol 2013; 31(2): 144–154.
32. Frigerio B, Fracasso G, Luison E, Cingarlini S, Mortarino M, Coliva A, Seregni E, Bombardieri E, Zuccolotto G, Rosato A, Colombatti M, Canevari S, Figini M. A single-chain fragment against prostate specific membrane antigen as a tool to build theranostic reagents for prostate cancer. Eur J Cancer 2013; 49(9): 2223–32.
33. Hillier S, Maresca K, Femia F, *et al*., Preclinical evaluation of novel glutamate-urea-lysine analogues that target prostate-specific membrane antigen as molecular imaging pharmaceuticals for prostate cancer. Cancer Res 2009; 69: 6932–6940.
34. Bacich DJ, Pinto JT, Tong WP, Heston WD. Cloning, expression, genomic localization, and enzymatic activities of the mouse homolog of prostate-specific membrane antigen/NAALADase/folate hydrolase. Mamm Genome 2001; 12: 117–123.
35. Xavier C, Vaneycken I, D'Huyvetter M, Heemskerk J, Keyaerts M, Vincke C, Devoogdt N, Muyldermans S, Lahoutte T, Caveliers V. Synthesis, preclinical validation, dosimetry, and toxicity of 68Ga-NOTA-Anti-HER2 nanobodies for iPET imaging of HER2 receptor expression in cancer. J Nucl Med 2013; 54(5): 776–84.
36. Broisat A, Hernot S, Toczek J, De Vos J, Riou LM, Martin S, Ahmadi M, Thielens N, Wernery U, Caveliers V, Muyldermans S, Lahoutte T, Fagret D, Ghezzi C, Devoogdt N. Nanobodies targeting mouse/human VCAM1 for the nuclear imaging of atherosclerotic lesions. Circulation Res 2012; 110: 927–937.
37. Saerens D, Pellis M, Loris R, Pardon E, Dumoulin M, Matagne A, Wyns L, Muyldermans S, Conrath K. Identification of a universal VHH framework to graft non-canonical antigen-binding loops of camel single-domain antibodies. J Mol Biol 2005; 352(3): 597–607.
38. Xavier C, Devoogdt N, Hernot S, Vaneycken I, D'Huyvetter M, De Vos J, Massa S, Lahoutte T, Caveliers V. Site-specific labeling of his-tagged nanobodies with ^{99}mTc: a practical guide. Meth Mol Biol 2012; 911: 485–490.
39. Loening AM, Gambhir SS. AMIDE: a free software tool for multimodality medical image analysis. Mol Imag 2003; 2: 131–137.